

Understanding the interface behavior and theoretical failure of beam-like topologically interlocked structures

Ioannis Koureas^a, Mohit Pundir^a, Shai Feldfogel^a, David S. Kammer^a

^a*Institute for Building Materials, ETH Zurich, Zurich, Switzerland*

Abstract

Topologically interlocked structures are architected by fitting together blocks that are constrained geometrically through contact and friction by their neighboring blocks. As long as the frictional strength is nowhere exceeded, the blocks stick against each other, allowing for large rotations. Once the interfacial stresses exceed the frictional strength, relative sliding between the blocks alters the structure's mechanical response. Improving the structural performance, precisely the strength and the toughness, has been one of the main focal points in the literature. However, many fundamental questions regarding the role and effect of the interface mechanisms (stick and slip) and rotation of the blocks have not been addressed yet. Here, we carry out a parametric analysis to understand the effect of Young's modulus, friction coefficient and geometry of the blocks on the dominance of the stick or slip governed mechanism. We combine analytical and computational tools to analyze the failure mechanisms and the response capacities of beam-like topologically interlocked structures. This is achieved using a finite element method coupled with a penalty-based approach for enforcing contact constraints along interfaces. We show that the combination of the structure's height and the friction coefficient controls whether the failure mechanism is slip-governed or stick-governed. Furthermore, we demonstrate that the sticking mechanism across all interfaces along with the rotation of the blocks dictates a saturation level to the mechanical performance of a given structure irrespective of geometric and material properties. This provides a theoretical upper bound for the structural response of topologically interlocked structures, and establishes a benchmark of achievable performance under idealistic conditions.

Keywords: Architected Structures, Frictional Contact, Stick-Slip Governed Failure, Saturation Level

1. Introduction

Topologically interlocked structures (TIS) are assemblies of building blocks that hold together due to the blocks' unique interlocking shapes – a very simple example is shown in Fig. 1, however many other configurations have been proposed in recent years [1, 2, 3, 4, 5, 6, 7]. The unbonded nature of the blocks in TIS enables frictional interactions between them, which provides the structure (Fig. 1b) with the capability of withstanding external loads. TIS have been shown to demonstrate very promising properties, including high toughness against failure for structures made from brittle material [4, 8, 9] and structural integrity despite partial failure (*e.g.*, missing blocks in plate-like TIS) [10]. However, TIS have not found widespread application in engineering because the mechanics of TIS is extremely complex including highly non-linear mechanisms such as friction, and hence we are not yet in a position to provide predictive design tools. To support the next step in the development of TIS, we are in dire need of a fundamental understanding of the mechanical behavior and failure of TIS.

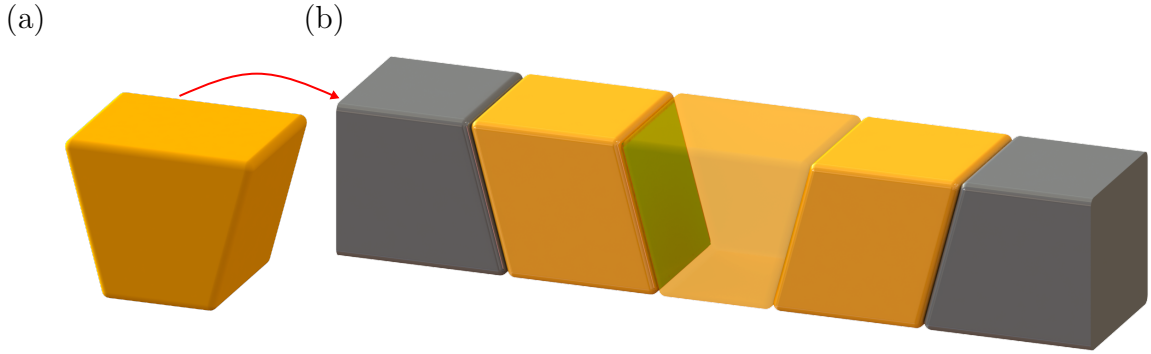


Figure 1: Topologically interlocked structure (TIS) made from truncated blocks. (a) Illustration of a single truncated block. (b) 3D illustration of assembling the blocks in a beam-like TIS as used in this study. The connected interfaces (green color) interlock the blocks with each other. The grey blocks serve as external support that holds the structure together.

While exploring the wide range of geometric configurations of TIS, recent experiments [9, 11, 12] showed that by subjecting TIS to external loads, the block interactions experience three distinct mechanisms, which are local slip, stick and rotation. Multiple mechanisms can but do not have to co-exist at any point in time or during the full failure process. Depending on the TIS design and material properties, these mechanisms take more or less prominent roles in governing the failure of the structure. However, it remains unclear how the TIS configuration results in the occurrence of these different block interactions, and how the latter – specifically the local stick-slip behavior – affects the global structural response (load-carrying capacity, initial stiffness, loading energy, and ultimate deflection).

Considering a situation where the stick mechanism is governing the mechanical response

of TIS, one can resort to analytical models, as, for instance, proposed in [11, 13, 14]. They modeled TIS as a truss, and derived the analytical expression for the horizontal and vertical reaction forces F_h and F_v at the local pivoting point A (Fig. 2a), which goes as follows:

$$F_v = F_h \left(\frac{h_{\text{eff}} - \delta}{l_{\text{eff}}} \right) = E\mathcal{A} \frac{l_{\text{eff}}}{\sqrt{l_{\text{eff}}^2 + h_{\text{eff}}^2}} \left(\frac{\sqrt{l_{\text{eff}}^2 + h_{\text{eff}}^2}}{\sqrt{l_{\text{eff}}^2 + (h_{\text{eff}} - \delta)^2}} - 1 \right) \left(\frac{h_{\text{eff}} - \delta}{l_{\text{eff}}} \right) \quad (1)$$

where E is the Young's modulus of the material, h_{eff} and l_{eff} are the effective height and length respectively (Fig. 2), \mathcal{A} the cross-sectional area of the truss between the pivoting points A and B, and δ the updated displacement ($\delta = u_y$, the applied displacement, if no slip occurred so far). Equation 1 clearly demonstrates that in a sticking situation the load-carrying capacity (*i.e.*, F_v) scales linearly with E and is strongly dependent on h_{eff} and l_{eff} . Furthermore, this expression can also qualitatively explain how local sliding reduces global stiffness by examining a specific slipped configuration. Specifically, when slip occurs¹, the initial pivoting point B moves to B' (Fig. 2b), reducing h_{eff} , l_{eff} , F_h , and hence the load-carrying capacity F_v (Equation 1). However, these observations remain qualitative, particularly regarding the stick-slip transition. Specifically, it remains unclear how local sliding occurs, and eventually leads to a global failure mechanism, which defines the carrying capacity of the structure.

Computational approaches, such as the finite element method (FEM), provide a great opportunity to model quantitatively the effects of local slip on the mechanical behavior of TIS. Particularly relevant to beam-like TIS, as studied here, is the work by Dalaq *et al.* [15] showing that the failure mode of architected beams depends on the number of blocks, friction coefficient and the shape of the interlocking interfaces. They showed that curved interfaces and smoothened corners promote sliding of the blocks and delay hinging (*i.e.*, stick and rotation) [16]. Their FEM analysis is in good quantitative agreement regarding the global load-displacement response - however, they focused on a specific material and did not investigate the effects of Young's modulus E , and block height h on the occurrence of stick, slip and rotation as block interactions, and their link to the mechanical response of the structures. Additionally, Zakeri *et al.* [17] showed that the height of TIS is a key parameter, and by increasing it, the initial stiffness and maximum load-carrying capacity of the structure increase. However, there is still no clear understanding of the relation of these material, geometric and friction properties with the presence of various block interactions, whether they promote a slip-governed or stick-governed failure mechanism,

¹Note that δ is being updated and corresponds to the loading since the last slip position as shown in Fig. 2b.

and how this affects the structural behavior such as the load-carrying capacity of TIS.

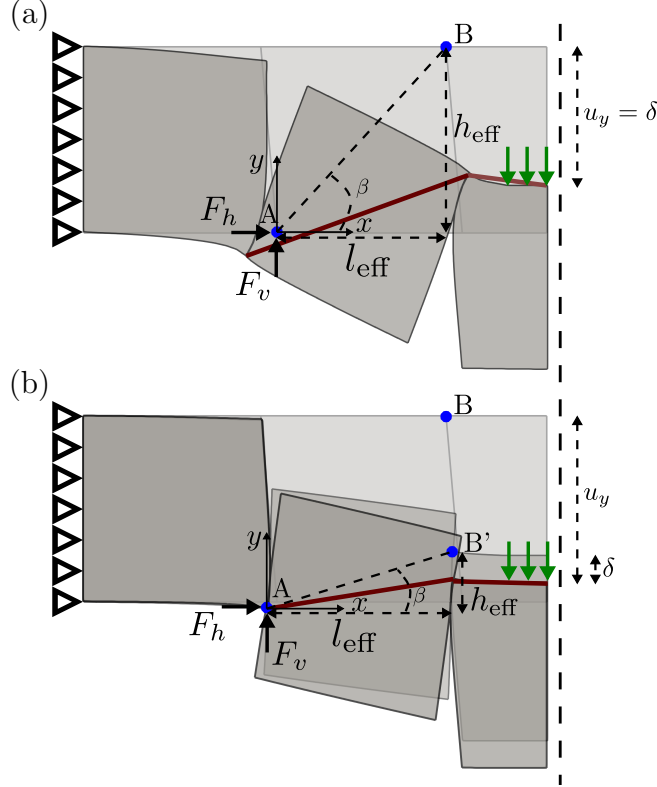


Figure 2: Equivalent truss model (dark red color) in a topologically interlocked structure (TIS). The effective height h_{eff} and length l_{eff} , as well as the displacement δ are shown for (a) stick and (b) slip TIS scenarios.

In this work, we aim to establish a fundamental understanding of how local mechanisms, such as the stick-slip transition at interfaces, affect the mechanical performance of TIS. While TIS have been studied in a large variety of geometric configuration, here, we deliberately consider one of the simplest TIS designs, which enable us to focus independently on the effects of material, geometry and friction. Specifically, we consider a topologically interlocked beam-like structure with a varying set of material properties (μ, E) and geometrical parameters (h). We will show how these parameters lead to stick, slip, and rotation at the interfaces between the building blocks, and collectively affect the response of TIS, such as the maximum load-carrying capacity, loading energy, initial stiffness and ultimate deflection. In particular, we will demonstrate that a complete sticking mechanism across all interfaces provides an upper bound to the maximum load-carrying capacity of a structure irrespective of geometric and material properties. Finally, we will outline and discuss ideas on how the gained knowledge can be used to optimize the structural performance of TIS.

Table 1: Symbols and notations

Symbol	Description	Unit
E	Young's modulus	N/m ²
F_a	Resultant force at a given pivoting point of the truss model	N
F_y	Load-carrying capacity of the structure	N
F_{\max}	Maximum load-carrying capacity of the structure	N
h	Height of a block (= structural depth)	m
h_{eff}	Effective height in a TIS	m
K_{TIS}	<i>Normalized</i> initial stiffness of the TIS	-
l	Length of a block	m
l_{eff}	Effective length in a TIS	m
L	Total length of a TIS	m
N	Normal force along a TIS interface	N
t	Thickness of a TIS	m
T	Tangential force along a TIS interface	N
u_y	Prescribed displacement at the top central surface of the middle block	m
U	Loading energy of the structure	Nm
β	Angle controlled by h_{eff} and l_{eff}	°
δ	Applied displacement based on the truss model	m
ε_n	Normal penalty parameter	N/m ³
ε_t	Tangential penalty parameter	N/m ³
θ	Truncated angle	°
μ	Friction coefficient	-
μ_{sat}	Saturated friction coefficient	-
ν	Poisson's ratio	-

2. Numerical Model

The examined configuration of beam-like TIS consisting of n building blocks is depicted in Fig. 3a. Each block is characterized by its truncated angle θ , height h and length l with an overall length L . The blocks are considered to be isotropic linear elastic material with Young's modulus E , Poisson's ratio ν and friction coefficient μ . A description of the symbol notation we use is provided in Table 1.

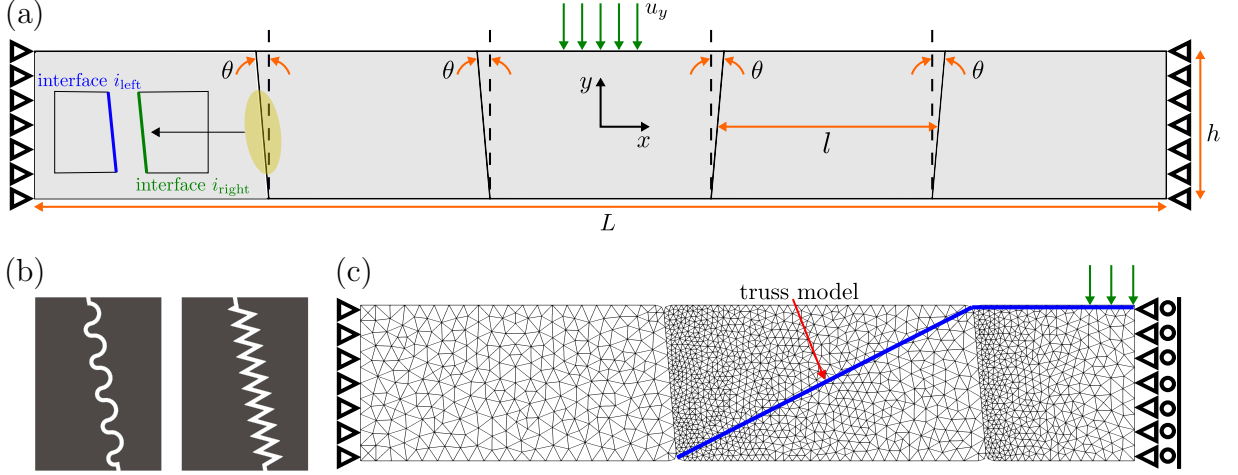


Figure 3: Schematic representation of model set-up showing (a) the geometric parameters and boundary conditions in a TIS with five blocks. Every structure consists of i interfaces where $i = 1, 2, \dots, k$ with k being the total number of interfaces in a structure. Every interface consists of two sides, the left and the right. (b) Schematic illustration of two rough surfaces that can be represented numerically by the friction coefficient μ . (c) Mesh and boundary conditions as used in the simulation. The blue line represents the truss model.

We use the FE method to solve the proposed model. We employ finite strain formulation to account for the large deformations and large rotations of the building blocks [18]. Thus, considering n deformable bodies Ω_n^i , the weak formulation at load increment i is described as:

$$\sum_{n=1}^n \int_{\Omega_n^i} \underline{\underline{\epsilon}}^i : \mathbb{C} : \delta \underline{\underline{\epsilon}}^i d\Omega_n^i + \sum_{n=1}^n \int_{\Omega_n^i} \underline{\underline{S}}^i : \delta \underline{\underline{\eta}} d\Omega_n^i = W_{\text{ext}}^{i+1} - \sum_{n=1}^n \int_{\Omega_n^i} \underline{\underline{S}}^i : \delta \underline{\underline{\epsilon}} d\Omega_n^i \quad (2)$$

where, $\underline{\underline{S}}$ and $\underline{\underline{\epsilon}}$ are the 2^{nd} Piola-Kirchhoff stress tensor and the linear strain tensor, respectively. W_{ext}^{i+1} is the virtual work of the external forces, $\underline{\underline{\eta}}$ represents the nonlinear incremental strain tensor and \mathbb{C} the 4^{th} order constitutive tensor. A node-to-segment contact algorithm, with penalty-based constraints, is employed [19, 20, 21, 22, 23] to enforce contact and frictional constraints along the interfaces of n deformable bodies. We use the penalty method for its computational simplicity. The virtual work δW_c of the contact forces at the current configuration for n deformable bodies that come in contact at k interfaces S_k is expressed as:

$$\delta W_c = \sum_{k=1}^k \int_{S_{k_{\text{slave}}}} (T_n \mathbf{n} + \mathbf{T}_t) \cdot (\delta \mathbf{u}_{k_{\text{slave}}} - \delta \mathbf{u}_{k_{\text{master}}}) dS_{k_{\text{slave}}} \quad (3)$$

where T_n is the traction along the normal \mathbf{n} to the interface and \mathbf{T}_t is the frictional traction tangential to \mathbf{n} integrated over one of the two contact surfaces termed as slave surface. Based on the penalty approach, $T_n = \varepsilon_n \langle g \rangle$ is approximated as a linear function of the

orthonormal gap between a slave node and the master surface. Similarly, $\mathbf{T}_t = \varepsilon_t(\Delta \mathbf{u}_t)$ is approximated as a linear function of the tangential slip distance ($\Delta \mathbf{u}_t$) between a slave node and the master surface, computed based on the covariant derivative approach [20, 24]. The penalty parameters ($\varepsilon_n, \varepsilon_t$) are area regularized to ensure that the computed contact forces are mesh independent [25, 26]. In order to overcome the biases in choosing a slave and master surface at an interface (see Equation 3), a two-pass algorithm [25, 26] is employed whereby at each load increment, the contact forces at a node are computed considering once a surface as a slave and then as a master. The FE code with the finite strain formulation and the node-to-segment contact algorithm, is developed as in-house code and has been validated for frictional cases (more details provided in Appendix A.1).

For the numerical analysis, the topologically interlocked beam (Fig. 1b) is modelled as a 2D structure under plane-strain conditions. The structure is discretized using first-order triangular elements (Fig. 3c), and the corners are rounded to overcome stress singularities. We exploit the symmetry of the structure along the y -axis and model half of the TIS. The left end is constrained in x and y directions, and at the right end, symmetric boundary conditions along the x direction are applied. A vertical displacement u_y is incrementally prescribed on the top boundary of the central block. All simulations are performed under static conditions.

For the parametric analysis, the influence of the geometry of the structure and the physical parameters are explored. L and l are kept constant and the values for E , μ and h are varied. The material and geometrical values used for the parametric analyses are presented in Table 2. We apply values of E that cover an essential range of brittle materials and allow us to study the effect of material elasticity on the structural stiffness of TIS. Furthermore, we explore a wide range of μ to understand the effect of interfacial friction of the blocks. Here, μ represents a combination of both a material parameter and a surface topology, *i.e.*, $\mu = \mu_{\text{mat}} + \mu_{\text{surf}}$. More specifically, a high μ can represent a rough surface with the complexity of the roughness at the interface being captured in the value of μ_{surf} (Fig. 3b). Explicit modeling of roughness goes beyond the scope of this work and is left for future studies. Further, we note that our model does not account for possible fracture of blocks, which could reduce the performance of TIS. However, our model provides an upper bound for the response capacities.

Table 2: Material parameters

Parameter	Value
E (GPa)	1, 2, 3, 10, 20, 30
h (mm)	1.0, 1.5, 2.0
l (mm)	2.0
L (mm)	10
t (mm)	1.0
θ ($^\circ$)	5
μ	0.2, 0.4, 0.6, 0.8, 1.0, 1.2
ν	0.2

To ensure that the FE framework can correctly capture the response of TIS, a three-dimensional experimental setup is considered, as well as its analytical solution [15]. Specifically, the behavior of a five-block pre-compressed structure with $\theta = 0^\circ$ is explored. The results show that the model compares qualitatively and quantitatively very well with the analytical model and reasonably well with the experiments (Fig. 4). This validation ensures that a 2D model gives the load response similar to a physical 3D structure.

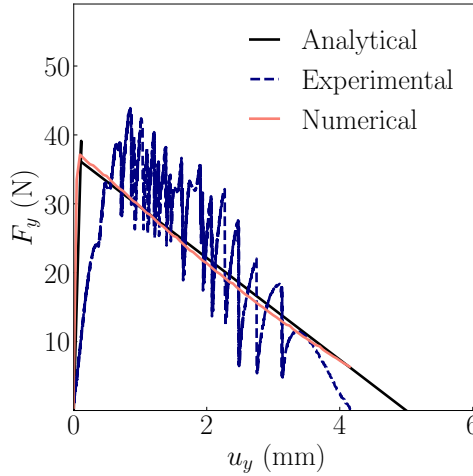


Figure 4: Load-carrying capacity F_y against the prescribed displacement u_y for a five-block pre-compressed structure with truncate angle $\theta = 0^\circ$. The experimental and analytical results have been taken from [15].

Since the considered beam-like TIS has at least one geometrically unconstrained block, the behavior of this block is highly dependent on the interfacial mechanism. Therefore, a correct resolution of interfacial mechanisms is critical for modeling a topologically inter-locked structure. A sensitivity analysis based on the global load response and the local interface mechanism is performed (see Appendix A.2). We chose mesh sizes and the penalty parameters such that both convergences are simultaneously reached.

3. Results and Discussion

3.1. Global Mechanical Response

In the simulations, the maximum load-carrying capacity F_{\max} is computed as the maximum value of F_y and the loading energy as $U = \int_0^{u_{\max}} \mathbf{F}(u_y) du_y$ with u_{\max} such that $\mathbf{F}(u_{\max}) = 0$ and $\left. \frac{\partial \mathbf{F}}{\partial u_y} \right|_{u_{\max}} < 0$. Since fracture is neglected, the failure of the structure is characterized by the central block being completely pushed out of the structure. The relation between F_{\max} , U , initial normalized stiffness (K_{TIS}) and ultimate deflection is investigated for the different structures with a focus on the underlying mechanisms causing these properties.

For all designs with different h , μ and E , the predicted $F_y - u_y$ curves are presented in Figure 5. F_y is normalized with respect to h , t and E while the deflection is normalized with respect to h to remove the scalability effect. In all cases, there is a non-monotonic behavior. The force initially increases linearly with the prescribed displacement. The initial slope of the normalized $F_y - u_y$ curves during the first 5% of the simulation gives K_{TIS} of the structure (Fig. 5a). It progressively deviates from the linear behavior and eventually reaches a peak value F_{\max} . Beyond that point, the force decreases until it reaches zero, where the central block is being pushed out of the structure. This behavior is similar to other TIS [12, 14].

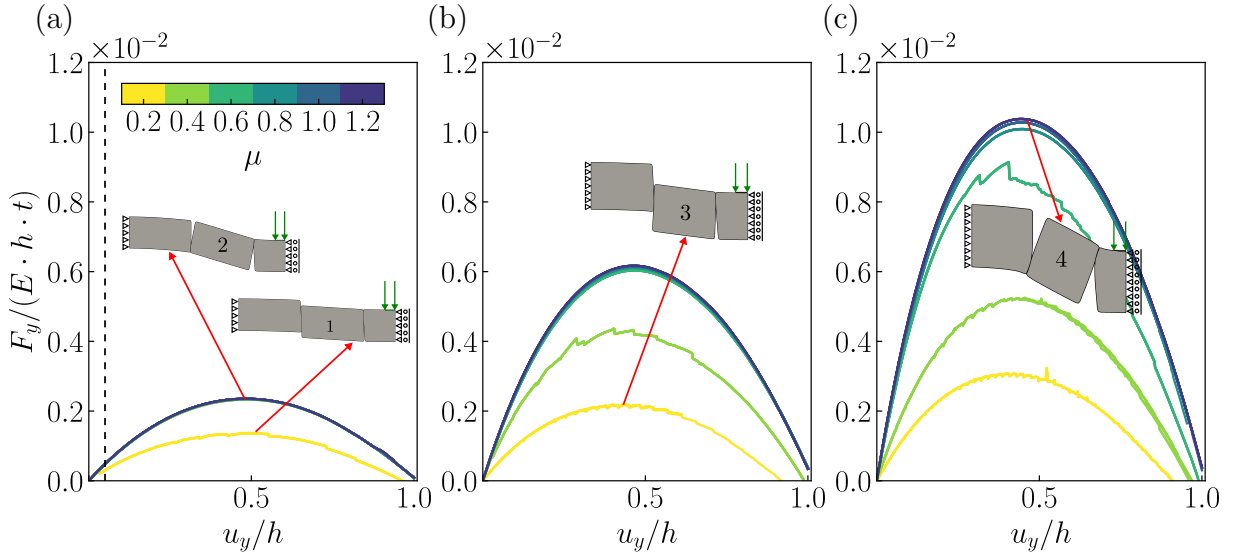


Figure 5: Load-carrying capacity F_y normalized with respect to the Young's modulus E , the height h and thickness t of the structure against the prescribed displacement u_y normalized with respect to the height h of the structure. The curves correspond to a structure truncated at an angle $\theta = 5^\circ$ with (a) $h = 1.0$ mm, (b) $h = 1.5$ mm and (c) $h = 2.0$ mm. The structures numbered 1 and 3 show cases where the sliding mechanism is observed while structures 2 and 4 show cases where the sticking mechanism is observed. The dashed horizontal black line represents the first 5% of the simulation which is used to compute the initial stiffness K_{TIS} .

From our analysis we observe that E does not affect the local interface mechanisms or the local behavior of the structure. However, the global mechanical response scales linearly with E irrespective of the friction coefficient. The presence of a linear relationship between E and mechanical response for such a wide range of friction coefficients is rather interesting. Such a linear dependency can be predicted for high values of μ , assuming that slipping is suppressed along the interfaces (see Equation 1 and [13]). However, for lower values of friction coefficient ($\mu = 0.2, 0.4$), where the slipping occurs, as will be shown later in the Section 3.2, such a linear dependency has not been shown. This means that E is the main material property that should be considered for controlling the response capacity of TIS.

The simulation results show that F_{\max} (Fig. 6a), U (Fig. 6b) and K_{TIS} (Fig. 6c) increase for increasing μ until a saturation level is reached. This occurs for all structures and for all values of E and h . As a result, we can say that for every structure there exists a saturated friction coefficient μ_{sat} for which any further increase for μ (i.e., $\mu > \mu_{\text{sat}}$) does not cause any further increase to the mechanical performance of the structure. For example for $h = 1.0$ mm, $\mu_{\text{sat}} = 0.4$. Similarly for $h = 1.5$ mm and $h = 2.0$ mm, $\mu_{\text{sat}} = 0.6$ and $\mu_{\text{sat}} = 0.8$, respectively (Fig. 6).

Moreover, we observe that by increasing h (for constant l) F_{\max} , U and K_{TIS} increase approximately linearly for $\mu \geq \mu_{\text{sat}}$ (Fig. 6). In addition, the ultimate deflection in a beam-like TIS without hierarchical levels cannot exceed the structure's height (h). This observation is also in agreement with the analytical expression from Equation 1. When the applied displacement becomes equal to the structure's height, the reaction force becomes 0 showing that the maximum deflection is equal to h . Therefore, μ , $\frac{h}{l}$ and E are the main parameters that affect the global response of TIS and ultimately F_{\max} , U , K_{TIS} and ultimate deflection.

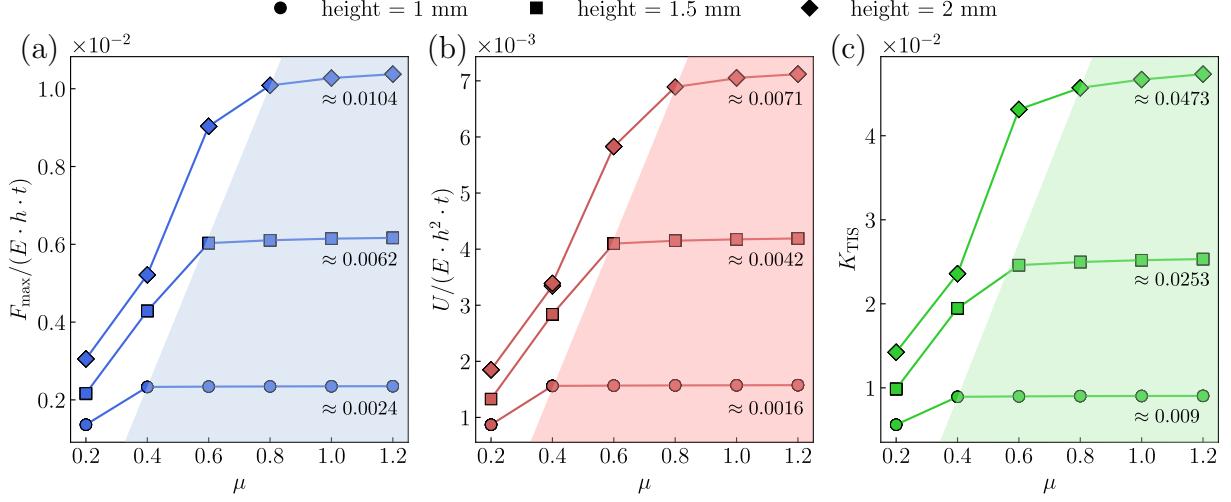


Figure 6: Overview of the mechanical performance of beam-like TIS. Showing the saturation for (a) the maximum load-carrying capacity F_{\max} , (b) the loading energy U normalized with respect to the Young's modulus E , the height h and thickness t of the structure and (c) the normalized initial stiffness K_{TIS} plotted against the friction coefficient μ for structures with $h = 1.0$ mm, $h = 1.5$ mm and $h = 2.0$ mm. By increasing μ the structure reaches a maximum value for all cases (see the approximated value). The lines have been added as a guide to the eye. The shaded areas signify the saturated regions.

3.2. Insights on Interface Mechanisms

The nature of TIS suggests that their mechanical performance is the direct result of interfacial mechanisms. To better understand the effect of TIS mechanisms on the mechanical behavior of the structure we deemed necessary to take a closer look at the interface between the blocks. In particular, we observe that the stick and slip interface mechanisms control the rotation mechanism of the blocks and ultimately the mechanical response of a structure.

First, we focus on the local response of the stick and slip mechanisms at every interface independently. We analyze the sliding percentage at every interface and load increment. When all nodes at a given interface slide, the entire interface is considered to slide. Otherwise, we can assume that the interface demonstrates local sticking mechanism. All interfaces need to present local sticking for a structure to stick (globally) at a given load increment. Figure 7 shows an example for a structure that demonstrates both mechanisms at different load increments. Initially the structure slides because interface 1 slides entirely. At some point (i.e. at $u_y/h = 0.35$), however, both interfaces stick locally (i.e., sliding percentage $< 100\%$) and therefore the whole structure sticks.

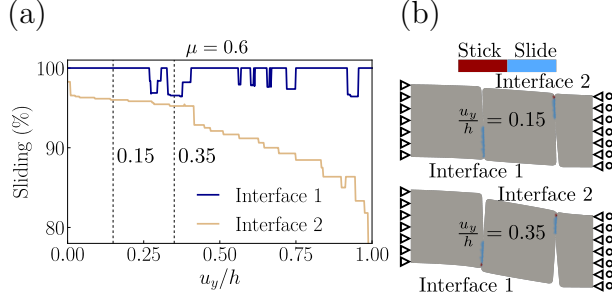


Figure 7: Interface mechanism. (a) Percentage of sliding against the prescribed normalized displacement u_y at every interface of a structure with height $h = 2$ mm and $\mu = 0.6$. (b) Snapshots capturing the sliding and sticking mechanisms at the interfaces of the structure at $\frac{u_y}{h} = 0.15$ and $\frac{u_y}{h} = 0.35$.

At the structural level, we consider the global sticking percentage, which is computed as the percentage of load increments at which a structure sticks at all interfaces during the simulation. Figure 8 segregates structures that remained stuck throughout the entire process and others that experienced at least some episodes of sliding (global not local). The results are compared with an analytical line derived from the truss model (Equation 1) marking the boundary between complete sticking and sliding. We derive a theoretical boundary that marks the global transition from sticking to a slipping regime by employing the truss model for TIS, as discussed in [13]), and Coulomb's friction law ($T = \mu N$). The tangential force T and the normal force N along an interface of TIS are computed by resolving F_v and F_h into F_a along a respective direction (β) as follows:

$$N = -\left(\left(\sin(\beta)\sin(\theta) + \cos(\beta)\cos(\theta)\right)F_a\right) \quad (4)$$

$$T = -\left(\left(\sin(\beta)\cos(\theta) - \cos(\beta)\sin(\theta)\right)F_a\right) \quad (5)$$

Angle β is controlled by h_{eff} and l_{eff} (Fig. 2). The expressions from (4) and (5) are substituted into the Coulomb friction model for computing μ_{sat} that controls the transition from sliding to global sticking:

$$T = \mu_{\text{sat}} N \implies \mu_{\text{sat}} = \frac{\sin(\beta)\cos(\theta) - \cos(\beta)\sin(\theta)}{\sin(\beta)\sin(\theta) + \cos(\beta)\cos(\theta)} \quad (6)$$

The results show a good agreement with the analytical prediction (Fig. 8). When the combination of h and μ for a given structure lies in the sticking regime (right side of the analytical solution), then the structure demonstrates the same global and local behavior. The interfaces present sticking mechanisms throughout the loading process, and as a result, the structure experiences saturation levels for F_{max} , U , K_{TIS} and maximum deflection. However, for all other cases, we observe sliding mechanism at some point which

reduces F_{\max} , U , K_{TIS} and maximum deflection. For example, when $\mu = 0.2$, sliding conditions are observed throughout the simulation, causing particularly low F_{\max} compared to the cases where a local sticking mechanism is presented throughout the simulation.

We also note that the increase of $\frac{h}{l}$ promotes sliding (Fig. 8). For a constant μ and l , as h increases, the magnitude and the direction of the thrust line changes, which alters the normal and tangential forces at the contact points. Based on Coulomb friction, a point is reached where the ratio between the tangential and normal forces exceeds the friction coefficient, and the structure starts sliding. Based on the results, but also from analytical expressions derived in the literature [13, 15], we find $K_{\text{TIS}} \propto \frac{h}{l}$. The smaller the $\frac{h}{l}$, the smaller the compression experienced by TIS and, therefore, the smaller the F_{\max} , U and K_{TIS} .

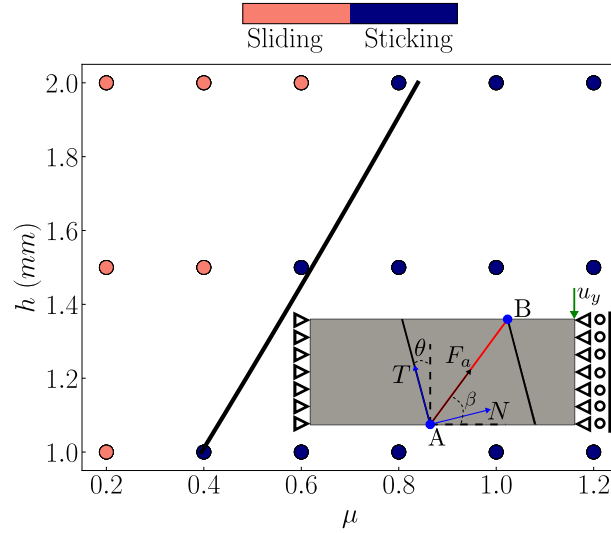


Figure 8: Global failure mechanism. Dark points correspond to setups that lead to failure governed by sticking, whereas light points correspond to setups that lead to slip-governed failure. The black line represents the boundary based on the analytical solution from the truss model (Equation 6).

While not all mechanisms (i.e., sliding, sticking and rotation) might be observed in a simulation, at least two must be present in TIS, with rotation of some of the blocks being a necessity for all models. By increasing μ , the blocks stick locally (at some load increments), which causes more rotation of the blocks (see Fig. 5 structures 2 and 4) compared to cases where there is sliding (see Fig. 5 structures 1 and 3). An increase in rotation of the blocks causes more compression and, therefore, the tangential force at the contact interface that is required for the transition from sticking to sliding changes. In some cases, this transition is never fulfilled, and the structure sticks, providing the strongest, stiffest and toughest scenario for a given configuration. In contrast, by increasing h , sliding is promoted, and a higher friction coefficient is required for the interfaces to stick. Increasing h implies higher K_{TIS} , F_{\max} and U because while the blocks rotate, higher compressive

forces are required for the central block to be pushed out of the device. By controlling these three mechanisms, K_{TIS} , F_{max} and U of the structure can be adjusted.

3.3. Capacity Saturation for other Geometries

Our work shows that the described beam-like structures reach theoretical maximum response capacities with μ_{sat} independently on the material properties (E) and geometrical parameters (h , l). This observation was obtained based on the behavior of blocks with planar interfaces. In order to examine the generality of the observation, we consider two additional cases with non-planar interfaces. Figure 9 shows the undeformed beam configurations with curved and kinked interfaces. The capacity saturation curves and a snapshot of the failure mechanism are shown for the two cases in Figure 9c and 9d. Like the blocks with planar interfaces, the load-carrying capacity attains saturation. However, for structures with curved interfaces, the saturation level required a greater μ (i.e., $\mu_{\text{sat}} = 2$) compared to the cases with straight interfaces (i.e., $\mu_{\text{sat}} = 0.8$). This observation is in agreement with Dalaq *et al.* [15], who showed that curved surfaces can promote sliding mechanism and delay sticking. Finally, we note that the use of curved surfaces reduces the value of the saturation level (i.e., $F_{\text{max}} \approx 0.007$ compared to $F_{\text{max}} \approx 0.01$) for the planar interfaces. In addition, sliding does not allow the structure to reach the maximum theoretical deflection. These findings are universal for any beam-like structure regardless of block geometry.

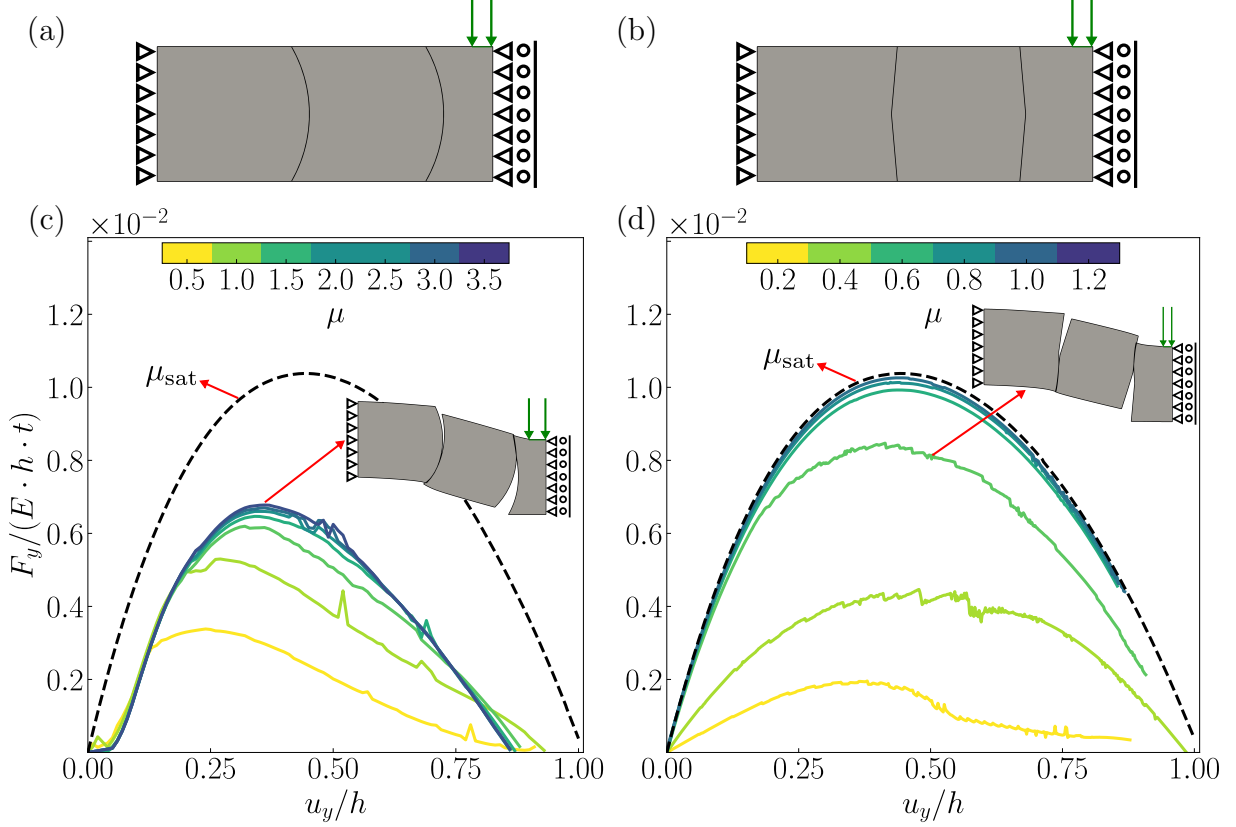


Figure 9: Beam-like TIS with (a) curved and (b) kinked interfaces. Load-carrying capacity F_y normalized with respect to the Young's modulus E , the length L and thickness t of the structure against the normalized prescribed displacement u_y . The curves correspond to (c) a five-block structure with curved interfaces and curvature ratio $c = \frac{l}{R} = 1$ with R being the radius of the curvature and (d) a five-block structure with kinked interfaces and truncated angle $\theta = 5^\circ$. The black dashed line corresponds to the equivalent saturated curve for five-block structure with planar interfaces and $\mu = 1.2$.

3.4. Saturated Friction Coefficient from a Design Perspective

In all analyses performed, the saturation level has been observed for high values of friction coefficient. We have used friction coefficients that are unrealistically high as a tool to model structured interfaces (e.g., roughness). Therefore, the complexity of the interface is simply described by friction coefficient. Even the smallest μ_{sat} in our models is a high value for typical materials. This raises questions with regard to the applicability of the saturation results and the ability to practically obtain the upper bound capacities discussed here. One way of attaining these upper bounds is through geometrically architected interfaces, such as the ones explained in Djumas *et al.* [27]. The interfaces of these structures are characterised by hierarchical levels. This would allow us to separate the effective friction coefficient into the contribution from the material μ_{mat} and the surface topology μ_{surf} . The hierarchical design would lead to high values for μ_{surf} , which would allow us to achieve an effective friction coefficient equal to μ_{sat} for realistic values of μ_{mat} . This shows that μ_{sat} and the upper bound for the structural load-carrying capacity

can be practically achieved through explicitly modeling of the interface geometry with hierarchical levels.

3.5. General Comments

In our study, fracture is not considered. We assumed that a structure fails when the central block is pushed out of the assembly. This is a realistic scenario for many configurations [28, 29, 30, 31], but may not cover all possible cases. It still leaves an open question regarding the precise moment where the onset of fracture in a load-deflection curve initiates. Moreover, fracture propagation, which depends on the interface geometry and interface mechanisms, could provide new insights into TIS’s mechanical performance. For instance, local fracture in a block may not lead to failure of the structure, but it can introduce new smaller bodies in the structure that entangles TIS’s mechanical response.

The sliding and rotation of the blocks are crucial for the mechanical behavior of TIS as it introduces a non-linear behavior in a structure made from linear elastic material. When sticking occurs, applied work is stored in the form of elastic energy [27, 32]. In that case K_{TIS} is controlled by E of the blocks, l_{eff} and h_{eff} . The structure can be described as elastic when the model is characterized by the stick and rotation mechanisms. As a result, the model is load independent. When sliding occurs, however, the structure becomes load-path dependent. The advantage of such a structure against a ductile material is that the building blocks do not physically undergo plastic deformation but only the structure. Moreover, it is possible to have a structure that initially sticks (behaves elastically) within the service range. However, it can also behave inelastically (through sliding) once it exceeds a specific value. Design parameters alongside material properties are considered as the main factors affecting the ultimate behavior of TIS. Therefore, we conclude that TIS made from linear elastic materials can express both elastic and inelastic behavior at the structural scale.

4. Conclusion

This study presented a parametric analysis of TIS to understand the various interfacial mechanisms governing the structural response of beam-like topologically interlocked structures. The stick and slip mechanisms limit the design span of these structures. When the sticking mechanism dominates, the structure’s response is mainly governed by the Young’s modulus and the height of the unconstrained blocks which dictates a saturation level to the initial stiffness, maximum load-carrying capacity, loading energy and ultimate deflection. When sliding occurs at interfaces, it decreases the effective height and effective length of the structure by shifting the local pivoting points which leads to a decrease in the maximum load-carrying capacity. The advantage of a sliding mechanism is that it

can potentially increase the serviceability of the structure providing a more sustainable design. Our study allows to identify the effect of the main geometrical, material and interfacial parameters on the slip-governed failure of topologically interlocked structures. Essentially, the ratio $\frac{h}{l}$ and E of the blocks control the mechanical response of the structure, while the μ and the interface geometry control the stick and slip governed failure mechanisms. Finally, E does not affect the failure mechanism of the structure, while by increasing $\frac{h}{l}$ sliding mechanism is promoted. Further improvement in the mechanical behavior of a TIS can be achieved by introducing hierarchical levels in the design. However, even if hierarchical levels characterize a structure, incorrect architecture can lead to ineffective utilization of the geometry. The insights of this study will serve as a baseline for examining and explaining the response of more complex structures.

Acknowledgements

We acknowledge Dr. Vladislav Yastrebov, MINES ParisTech for the helpful discussions.

Appendix A.

Appendix A.1. Validation of Frictional Contact

Since the behavior and failure of TIS completely depends on friction resistance and stick and slip mechanisms, the accuracy of the results depend entirely on the validity of the contact formulation. As further validation of the frictional contact, the Cattaneo and Mindlin's problem is considered. This benchmark involves two elastic cylinders that are pressed together. The bottom half-cylinder has its base constrained in the vertical and horizontal direction while the top surface of the top half cylinder is displaced by u_x and u_y (Fig. A.10a). The normal T_n and tangential T_t tractions along the contact surface are computed and plotted together with the analytical solution. For computing the analytical solution, the normal F_n and tangential F_t reaction forces are calculated from the surface where the prescribed displacement is applied. Using the analytical solution [33] T_n and T_t are computed as:

$$T_n(x) = \frac{2F_n\sqrt{\alpha^2 - x^2}}{\pi\alpha^2} \quad (\text{A.1})$$

$$T_t(x) = \frac{2\mu_s F_n}{\pi\alpha^2} \left[\sqrt{a^2 - x^2} - H(c^2 - x^2)\sqrt{c^2 - x^2} \right], \quad -\alpha < x < \alpha \quad (\text{A.2})$$

where,

$$\alpha = \left[\frac{4F_n R_0 R_1}{\pi(R_0 + R_1)} \left(\frac{1 - \nu_0^2}{E_0} + \frac{1 - \nu_1^2}{E_1} \right) \right]^{\frac{1}{2}} \text{ and } c = \alpha \left(1 - \frac{F_t}{\mu_s F_n} \right)^{\frac{1}{2}} \quad (\text{A.3})$$

Here, $H(\cdot)$ denotes the Heaviside function. A friction coefficient $\mu_s = 0.5$ is used and penalty parameters $\varepsilon_n = \varepsilon_t = 10^{12} \text{ N/m}^3$. The numerical results of T_t (Fig. A.10b) and

T_n (Fig. A.10c) are in good agreement with the results from the analytical solution.

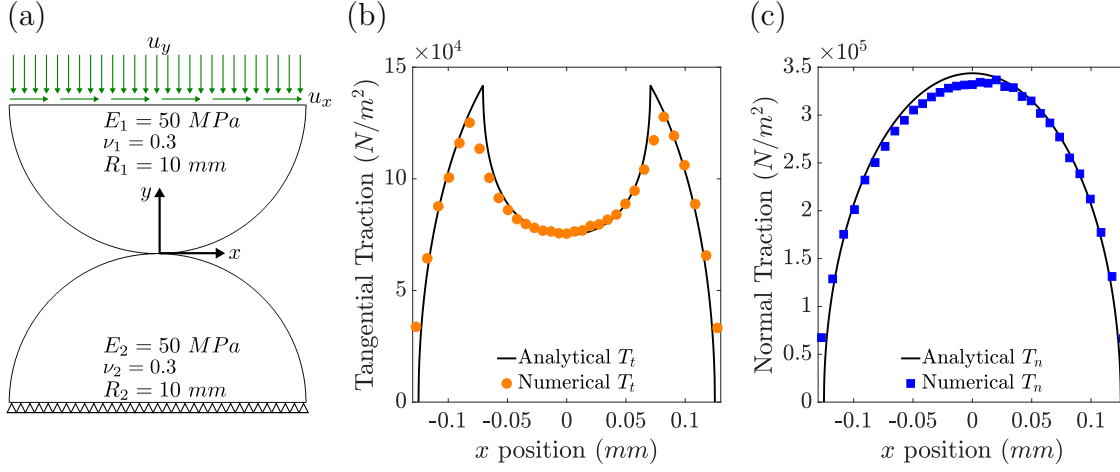


Figure A.10: Benchmark with the Cattaneo and Mindlin's problem. (a) Schematic setup showing the geometry of the half-cylinders, the boundary conditions applied and the material properties used in the simulation. Distribution of (b) T_t and (c) T_n as computed numerically (circles and squares respectively) and in comparison with the analytical solution (solid black lines) for friction coefficient $\mu_s = 0.5$.

Appendix A.2. Convergence Analysis

For the convergence analysis a five-block structure is used, with $\theta = 5^\circ$, $E = 1$ GPa, $h = l = 2$ mm and $\mu = 0.6$. The normalized $F_y - u_y$ response is examined for different mesh densities (Fig. A.11a). In all cases, the mesh density on one of the two surfaces at an interface is kept finer. The results from the $F_y - u_y$ curves are very similar and independent of the chosen mesh densities. The chosen mesh density is based on the fact that a sufficient number of nodes at the interface is needed to properly capture stick and slip mechanisms, but also to ensure reasonable computational cost. The chosen mesh density is then tested for different penalty parameters ε_n and ε_t (Fig. A.11b). The chosen penalty parameters do not affect the $F_y - u_y$ response. Moreover, it is tested that the penetration ξ of a slave node is small enough such that $\frac{\xi}{h} < 1\%$ (Fig. A.11c). Finally, ε_n and ε_t are kept constant at a given surface.

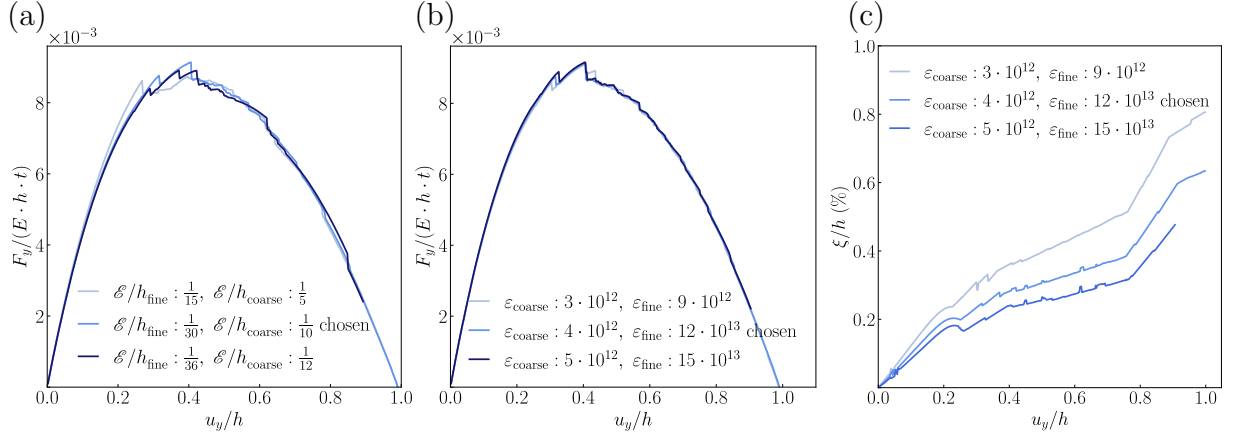


Figure A.11: Convergence analysis. Load-carrying capacity F_y normalized with respect to the Young's modulus E , the length L and thickness t of the structure against the normalized prescribed displacement u_y . The curves correspond to (a) different mesh densities and (b) different penalty parameters. (c) The chosen penalty parameters are tested to ensure $\frac{\xi}{h} < 1\%$.

References

- [1] A. V. Dyskin, Y. Estrin, A. J. Kanel-Belov, E. Pasternak, A new concept in design of materials and structures: Assemblies of interlocked tetrahedron-shaped elements, *Scripta Materialia* 44 (12) (2001) 2689–2694, 2001. doi:10.1016/S1359-6462(01)00968-X.
- [2] A. V. Dyskin, Y. Estrin, A. J. Kanel-Belov, E. Pasternak, Toughening by fragmentation-how topology helps, *Advanced Engineering Materials* 3 (11) (2001) 885–888, 2001. doi:10.1002/1527-2648(200111)3:11<885::AID-ADEM885>3.0.CO;2-P.
- [3] P. Y. Chen, A. Y. Lin, Y. S. Lin, Y. Seki, A. G. Stokes, J. Peyras, E. A. Olevsky, M. A. Meyers, J. McKittrick, Structure and mechanical properties of selected biological materials, *Journal of the Mechanical Behavior of Biomedical Materials* 1 (3) (2008) 208–226, 2008. doi:10.1016/j.jmbbm.2008.02.003.
- [4] L. Djumas, A. Molotnikov, G. P. Simon, Y. Estrin, Enhanced Mechanical Performance of Bio-Inspired Hybrid Structures Utilising Topological Interlocking Geometry, *Scientific Reports* 6 (January) (2016) 1–10, Nature Publishing Group, 2016. doi:10.1038/srep26706.
- [5] Z. Yin, F. Hannard, F. Barthelat, Impact-resistant nacre-like transparent materials 1263 (June) (2019) 1260–1263, 2019.
- [6] A. V. Dyskin, Y. Estrin, A. J. Kanel-Belov, E. Pasternak, Topological interlocking of platonic solids: A way to new materials and structures, *Philosophical Magazine Letters* 83 (3) (2003) 197–203, 2003. doi:10.1080/0950083031000065226.
- [7] S. Schaare, A. V. Dyskin, Y. Estrin, S. Arndt, E. Pasternak, A. Kanel-Belov, Point loading of assemblies of interlocked cube-shaped elements, *International Journal of Engineering Science* 46 (12) (2008) 1228–1238, Elsevier Ltd, 2008. doi:10.1016/j.ijengsci.2008.06.012.
- [8] M. Mirkhalaf, A. K. Dastjerdi, F. Barthelat, Overcoming the brittleness of glass through bio-inspiration and micro-architecture, *Nature Communications* 5 (2014) 1–9, Nature Publishing Group, 2014. doi:10.1038/ncomms4166.
- [9] M. Mirkhalaf, T. Zhou, F. Barthelat, Simultaneous improvements of strength and toughness in topologically interlocked ceramics, *Proceedings of the National Academy of Sciences of the United States of America* 115 (37) (2018) 9128–9133, 2018. doi:10.1073/pnas.1807272115.

- [10] A. V. Dyskin, Y. Estrin, E. Pasternak, H. C. Khor, A. J. Kanel-Belov, Fracture resistant structures based on topological interlocking with non-planar contacts, *Advanced Engineering Materials* 5 (3) (2003) 116–119, 2003. doi:10.1002/adem.200390016.
- [11] S. Khandelwal, T. Siegmund, R. J. Cipra, J. S. Bolton, Adaptive mechanical properties of topologically interlocking material systems, *Smart Materials and Structures* 24 (4), IOP Publishing, 2015. doi:10.1088/0964-1726/24/4/045037.
- [12] M. Mirkhalaf, A. Sunesara, B. Ashrafi, F. Barthelat, Toughness by segmentation: Fabrication, testing and micromechanics of architected ceramic panels for impact applications, *International Journal of Solids and Structures* 158 (2019) 52–65, Elsevier Ltd, 2019. doi:10.1016/j.ijsolstr.2018.08.025.
- [13] S. Khandelwal, T. Siegmund, R. J. Cipra, J. S. Bolton, Scaling of the elastic behavior of two-dimensional topologically interlocked materials under transverse loading, *Journal of Applied Mechanics, Transactions ASME* 81 (3) (2014) 1–9, 2014. doi:10.1115/1.4024907.
- [14] S. Khandelwal, T. Siegmund, R. J. Cipra, J. S. Bolton, Transverse loading of cellular topologically interlocked materials, *International Journal of Solids and Structures* 49 (18) (2012) 2394–2403, Elsevier Ltd, 2012. doi:10.1016/j.ijsolstr.2012.04.035.
- [15] A. S. Dalaq, F. Barthelat, Strength and stability in architected spine-like segmented structures, *International Journal of Solids and Structures* 171 (2019) 146–157, Elsevier Ltd, 2019. doi:10.1016/j.ijsolstr.2019.04.012.
- [16] A. S. Dalaq, F. Barthelat, Manipulating the geometry of architected beams for maximum toughness and strength, *Materials and Design* 194 (2020) 108889, Elsevier Ltd, 2020. doi:10.1016/j.matdes.2020.108889.
- [17] M. Zakeri, M. Majidi, M. Haghighi-Yazdi, M. Safarabadi, Numerical analysis of linear and nonlinear buckling instability of plates made of topologically interlocked materials, *Mechanics Based Design of Structures and Machines* 0 (0) (2021) 1–13, Taylor & Francis, 2021. doi:10.1080/15397734.2021.1921596.
- [18] K.-J. Bathe, E. Ramm, E. L. Wilson, Finite element formulations for large deformation dynamic analysis, *International Journal for Numerical Methods in Engineering* 9 (2) (1975) 353–386, 1975. doi:10.1002/nme.1620090207.

- [19] A. Konyukhov, K. Schweizerhof, Contact formulation via a velocity description allowing efficiency improvements in frictionless contact analysis, *Computational Mechanics* 33 (3) (2004) 165–173, 2004. doi:10.1007/s00466-003-0515-3.
- [20] A. Konyukhov, K. Schweizerhof, Covariant description for frictional contact problems, *Computational Mechanics* 35 (3) (2005) 190–213, 2005. doi:10.1007/s00466-004-0616-7.
- [21] T. A. Laursen, *Computational Contact and Impact Mechanics*, Springer Berlin Heidelberg, Berlin, Heidelberg, 2003. doi:10.1007/978-3-662-04864-1.
- [22] P. Wriggers, T. A. Laursen, *Computational Contact Mechanics CISM Courses and Lectures*, vol. 498 498, 2007.
- [23] G. Zavarise, L. De Lorenzis, The node-to-segment algorithm for 2D frictionless contact: Classical formulation and special cases, *Computer Methods in Applied Mechanics and Engineering* 198 (41-44) (2009) 3428–3451, Elsevier B.V., 2009. doi:10.1016/j.cma.2009.06.022.
- [24] P. Wriggers, L. Krstulovic-Opara, J. Korelc, Smooth C1-interpolations for two-dimensional frictional contact problems, *International Journal for Numerical Methods in Engineering* 51 (12) (2001) 1469–1495, 2001. doi:10.1002/nme.227.
- [25] N. El-Abbasi, K. J. Bathe, Stability and patch test performance of contact discretizations and a new solution algorithm, *Computers and Structures* 79 (16) (2001) 1473–1486, 2001. doi:10.1016/S0045-7949(01)00048-7.
- [26] G. Zavarise, L. De Lorenzis, A modified node-to-segment algorithm passing the contact patch test, *International Journal for Numerical Methods in Engineering* 79 (4) (2009) 379–416, 2009. doi:10.1002/nme.2559.
- [27] L. Djumas, G. P. Simon, Y. Estrin, A. Molotnikov, Deformation mechanics of non-planar topologically interlocked assemblies with structural hierarchy and varying geometry, *Scientific Reports* 7 (1) (2017) 1–11, Springer US, 2017. doi:10.1038/s41598-017-12147-3.
- [28] I. A. Malik, F. Barthelat, Toughening of thin ceramic plates using bioinspired surface patterns, *International Journal of Solids and Structures* 97-98 (2016) 389–399, Elsevier Ltd, 2016. doi:10.1016/j.ijsolstr.2016.07.010.
- [29] I. A. Malik, M. Mirkhalaf, F. Barthelat, Bio-inspired “jigsaw”-like interlocking sutures: Modeling, optimization, 3D printing and testing, *Journal of the Mechanics*

- and Physics of Solids 102 (2017) 224–238, Elsevier Ltd, 2017. doi:10.1016/j.jmps.2017.03.003.
- [30] I. A. Malik, F. Barthelat, Bioinspired sutured materials for strength and toughness: Pullout mechanisms and geometric enrichments, International Journal of Solids and Structures 138 (2018) 118–133, Elsevier Ltd, 2018. doi:10.1016/j.ijsolstr.2018.01.004.
- [31] W. Wang, Y. Sun, Y. Lu, J. Wang, Y. Cao, C. Zhang, Tensile behavior of bio-inspired hierarchical suture joint with uniform fractal interlocking design, Journal of the Mechanical Behavior of Biomedical Materials 113 (March 2020) (2021) 104137, Elsevier Ltd, 2021. doi:10.1016/j.jmbbm.2020.104137.
- [32] T. Krause, A. Molotnikov, M. Carlesso, J. Rente, K. Rezwan, Y. Estrin, D. Koch, Mechanical properties of topologically interlocked structures with elements produced by freeze gelation of ceramic slurries, Advanced Engineering Materials 14 (5) (2012) 335–341, 2012. doi:10.1002/adem.201100244.
- [33] J. R. Barber, Elasticity, Vol. 172 of Solid Mechanics and Its Applications, Springer Netherlands, Dordrecht, 2010. doi:10.1007/978-90-481-3809-8.